

Image-Based BRDF Measurement Including Human Skin

Stephen R. Marschner* Stephen H. Westin Eric P. F. Lafortune
Kenneth E. Torrance Donald P. Greenberg

Program of Computer Graphics
Cornell University

Abstract: We present a new image-based process for measuring the bidirectional reflectance of homogeneous surfaces rapidly, completely, and accurately. For simple sample shapes (spheres and cylinders) the method requires only a digital camera and a stable light source. Adding a 3D scanner allows a wide class of curved near-convex objects to be measured. With measurements for a variety of materials from paints to human skin, we demonstrate the new method's ability to achieve high resolution and accuracy over a large domain of illumination and reflection directions. We verify our measurements by tests of internal consistency and by comparison against measurements made using a gonioreflectometer.

1 Introduction

To render accurate images reliably and easily, the reflectance of surfaces must be simulated accurately. The most direct way to ensure correct simulation is to use physical reflectance measurements. Such measurements can guide the choice of parameters for existing reflectance models, and if they are sufficiently complete they can be used as input for renderers or provide the basis for entirely new models. To completely capture the reflectance of an opaque surface, one must measure the *bidirectional reflectance distribution function* (BRDF). BRDF measurements have traditionally been made with purpose-built devices known as *gonioreflectometers*, which are rare and expensive.

This paper presents a system that measures reflectance quickly and completely without special equipment. The method works by taking a series of photographs of a curved object; each image captures light reflected from many differently oriented parts of the surface. By using a curved test sample and an imaging detector, and by using automated photogrammetry to measure the camera position, we eliminate the precise mechanisms needed to position the source and detector in a conventional gonioreflectometer. By knowing the sample shape and the light source position, we can analyze the photographs to determine the sample's BRDF. With only a light source and a digital camera, objects of known, regular shape can be measured; adding a 3D geometry scanner extends the technique to cover a whole class of surfaces, including human skin, that are impractical to measure by other methods. Although the apparatus is simple and the measurement rapid, the resulting data are accurate and can be very complete, covering the full hemisphere almost to grazing angles.

2 BRDF Background

The BRDF, f_r , completely describes the reflectance of an opaque surface at a single point. Its value measures the ratio of the radiance L exiting the surface in a given

*Current address: Microsoft Research, One Microsoft Way, Redmond, WA 98052-6399

direction to the incident irradiance I at a particular wavelength λ from an incident solid angle $d\omega_i$ about a given illumination direction. Representing the incident and exitant directions in spherical coordinates according to Figure 1,

$$f_r(\theta_i, \phi_i, \theta_e, \phi_e, \lambda) = \frac{dL(\theta_e, \phi_e)}{dI(\theta_i, \phi_i)}. \quad (1)$$

The BRDF is thus a function of five variables, but its domain is reduced somewhat by a symmetry called *reciprocity*, which states that reversing the light's path does not change the reflectance:

$$f_r(\theta_1, \phi_1, \theta_2, \phi_2, \lambda) = f_r(\theta_2, \phi_2, \theta_1, \phi_1, \lambda).$$

In this paper we will concentrate on the important class of *isotropic* materials, for which the reflectance is independent of rotating the incident and exitant directions about the surface normal. For these surfaces, the BRDF depends only on $\Delta\phi = \phi_e - \phi_i$, rather than on ϕ_i and ϕ_e separately, which reduces the domain from five to four variables:

$$f_r(\theta_i, \phi_i, \theta_e, \phi_e, \lambda) = f_r(\theta_i, \theta_e, \Delta\phi, \lambda). \quad (2)$$

In computer graphics, the wavelength dependence of BRDF is of interest only for the purposes of determining colors seen by human observers, so the continuous wavelength dimension can often be replaced with an appropriate discrete set of three measurements (R, G, B), further reducing the isotropic BRDF to a vector-valued function of three variables.

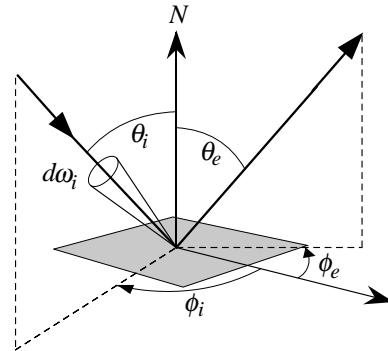


Fig. 1. Geometry of surface reflection.

3 Overview of Method

A straightforward device for measuring isotropic BRDFs is shown in Figure 2a, illustrating the three mechanical degrees of freedom required. A flat sample is illuminated by a light source, and a detector measures the complete distribution of reflected light by moving around the entire hemisphere. To measure a full BRDF, this process must be repeated many times, moving the light source each time to measure a different incidence angle.

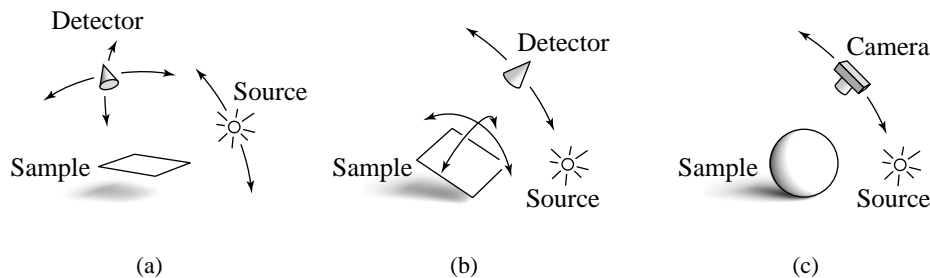


Fig. 2. Three BRDF measurement devices, including our image-based approach (c).

Because only the relative positions of the sample, source, and detector are relevant, all the same measurements could be made using the device of Figure 2b, in which the sample rotates with two degrees of freedom but the detector has only one and the source is fixed. The number of degrees of freedom remains the same, and all the same configurations of source, sample, and detector can be achieved.

If we replace the flat sample with a curved one, we can acquire data from many sample orientations simultaneously. Since every part of the sample's surface has a different orientation, we can use a camera to measure different parts of the surface instead of rotating the sample, as shown in Figure 2c. In this device, the two dimensions of the image sensor substitute for the two degrees of freedom of sample rotation. If there is sufficient curvature, we can make all the same measurements as the other devices, and by measuring two degrees of freedom in parallel we can greatly reduce the measurement time while increasing the sampling density.

This is the essence of image-based BRDF measurement: in an image of a curved object taken using a small light source, every pixel is in effect a BRDF measurement. Given a 3D model of the sample, camera, and light source, we can determine the incident and exitant directions for each pixel relative to the surface normal, as well as the irradiance due to the light source. Together with the radiance measured by the camera, these are all the data required to compute the BRDF.

Because a single image will only cover a two-dimensional subset of the possible BRDF configurations, many images are required to measure the whole domain. In the case of an isotropic BRDF, we are filling up the three-dimensional domain of the BRDF by measuring two-dimensional sheets, so we will need a one-dimensional sequence of images, with the camera or light source positioned differently in each.

4 Related Work

Traditionally [19,21], the three or four angular dimensions of the BRDF are handled by specialized mechanisms that position a light source and a detector at various directions from a flat sample of the material to be measured. Because three or four dimensions must be sampled sequentially, reflectance measurements are time-consuming, even with modern computer controls. Even a sparse sampling of the incident and exitant hemispheres can take several hours.

More recently, image-based methods have been used to speed measurements by gathering many angular samples at once. These methods, including the method presented in this paper, use a two-dimensional detector—the image sensor of a digital camera—to measure a two-dimensional range of angles simultaneously, leaving one or two dimensions of angle to be sampled by sequential measurements.

These can be categorized in two groups: those that attempt to measure the BRDF over its entire bihemispherical domain and those that measure some useful subset. The BRDF over an appropriate subset of the domain can be used to deduce characteristics of the surface microgeometry or to find parameters for a low-dimensional BRDF model.

One example of measuring a subset of the domain is the work of Karner et al. [15], who use images of a planar sample to measure the BRDF over a limited range of interesting angles. They use these data to fit coefficients for a simple reflectance model.

Ikeuchi and Sato [14] estimate reflectance model parameters using a surface model from a range scanner and a single image from a video camera. They use a curved sample to capture a larger range of incidence and exitance angles, but their data are still constrained to the angles provided by the illumination and view directions of a single image. Sato et al. [20] extend this method to deal with spatial variations in BRDF by

acquiring a sequence of images while the sample rotates. The image sequence provides samples along a one-dimensional path for each surface point; a simple reflectance model is fit to these data.

The surface optics literature also includes a number of approaches to measure a subdomain of the BRDF rapidly; these are generally used to deduce physical parameters of the surface itself, such as feature size on integrated circuits [12] or surface roughness [3], and often measure only at a single wavelength.

Ward describes a device [23] that is able to measure the complete BRDF of anisotropic materials. His camera captures the entire exitant hemisphere at once with a hemispherical mirror and a fisheye lens. The source and sample are moved mechanically to cover all incident angles.

More recently, Lu, Koenderink, and Kappers [17] use a cylindrical sample to give broad angular coverage in the incident plane, using multiple images with different source positions to cover all angles.

Like these other image-based systems, the system presented in this paper uses a camera to sample a two-dimensional set of angles in a single measurement, so it shares their advantages in speed and sampling density over traditional approaches. It can be thought of as a combination and extension of the techniques of Ward and Lu et al. By adopting a curved sample, it avoids the fisheye lens and hemispherical mirror of Ward’s method and permits measurements much closer to grazing.¹ By using samples with compound curvature, we extend coverage from the incidence plane to the entire BRDF domain. We go beyond both of these techniques in allowing hand-held positioning, which obviates any precision source positioning mechanism, and in extending the technique to arbitrary convex objects. The method of this paper was derived from that in the dissertation of the first author [18], but it works with more general shapes, requires less equipment, and is simpler to use.

The following sections describe the specifics of our system, give the results of measuring several materials, and demonstrate the accuracy of those results by comparing them to measurements from a gonireflectometer of verified accuracy.

5 Method

Our image-based technique can measure the BRDF of two different classes of objects: simple geometric shapes, for which the 3D shape can be defined analytically, and irregular shapes, for which the 3D model is provided by a range scanner.

Geometric shapes, such as spheres and cylinders, can be modeled and aligned precisely, giving measurements with low error. This approach also requires less equipment, since a range scanner is not required. However, only certain materials can be measured using these shapes—typically only paints or other man-made finishes that can be applied to such an object.

If a 3D description of the sample shape is available, we can measure any convex object that has a uniform BRDF. Since we no longer have to control the geometry, it becomes possible to measure many more interesting materials. This generality has a cost, however: the limitations of the scanner introduce geometric errors that lead to noise in our results.

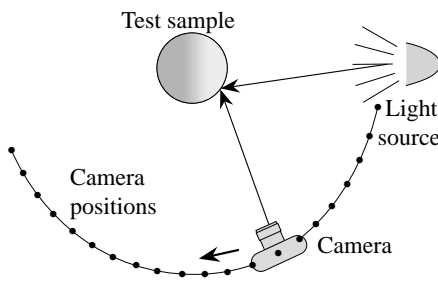


Fig. 3. Schematic of measurement setup.

¹Ward’s device covers angles of up to 45° to 75°, depending on azimuth angle [10].

We use a hand-held camera to photograph the sample from a sequence of positions, with a single stationary light source providing the only illumination. The camera moves from a position next to the light source, which allows measurement of near-retroreflection, to opposite the light source, where we measure grazing-angle reflection (Figure 3). A few additional photographs, described below, are also taken to measure the location and intensity of the light source. In all, a typical measurement session, including the range scan and all the photographs, takes about half an hour.

The equipment we use to make our measurements includes:

- A digital still camera using a 1.5 megapixel CCD sensor with an RGB color filter array (Kodak DCS 420).
- A simple industrial electronic flash, rated at 400 W-sec output (Photogenic Machine Co. EP377).
- A structured-light range scanner, for measurements of irregularly-shaped samples (Cyberware 3030/PS).

From each pixel in each measurement image we derive one sample somewhere in the domain of the BRDF; the locations of the samples are determined by the geometry of the sample’s surface and the arrangement of camera, source, and sample. As explained in Section 3, each image measures a two-dimensional set of BRDF configurations, but we take multiple images (typically about 30) from different positions to cover the full three-dimensional BRDF.

5.1 Calibration

Turning the camera images into accurate BRDF measurements requires both geometric and radiometric calibration. Geometric calibration establishes the relative positions of the light source, sample, and camera for each measurement image, and radiometric calibration determines the irradiance due to the source and the relationship between pixel values and radiance reflected from the sample.

Geometric calibration. Geometric calibration is done with photogrammetric techniques, using machine-readable targets that are placed on a structure positioned near the sample [18 (Appendix C)]. These targets are located and identified automatically in each image using ID codes embedded in the targets. The information that must be derived from the target locations includes:

- The position of the light source.
- The camera pose for each measurement image.
- The pose of the sample.

The poses of the camera are found from the image-plane target locations using bundle adjustment² [4, 7, 18 (Appendix B)]. Since our targets are recognized automatically and coded with unique ID numbers, no manual intervention is needed to establish correspondence between points in the various images.

There are three sets of targets: the *sample targets*, fixed with respect to the sample, the *source targets*, fixed with respect to the source, and the *stationary targets*, fixed in the room. The positions of the camera in the room are obtained using the stationary

²Bundle adjustment takes the image-plane projections of m points in n images and computes the m 3D locations of the points and the n camera poses by solving a nonlinear system of equations.

targets. Three extra images that include both the stationary targets and the source targets allow us to extract the position of the source in the room. The sample targets are used to determine the position of the sample relative to the camera positions. With the knowledge of these three relationships, the incident and exitant directions relative to the surface normal can be computed for any point on the sample. When measuring the skin of a human subject, which may change position from one image to the next (see Section 6.4), the sample position is determined separately for each frame, but when measuring inanimate samples the stationary targets are redundant, and are used only to improve position estimates. Gortler et al. [9] also used encoded targets to determine camera pose, but we have extended the technique to find sample and source positions; we also use more targets to cover a wide angular range robustly.

Radiometric calibration. In order to make BRDF measurements for each pixel, we must know the radiance reflected to the camera and the irradiance due to the source. To use a digital camera to measure radiance we must characterize both the optoelectronic conversion function (OECF), which relates the digital count reported for a pixel with the image-plane exposure, and the flat-field response, which relates the image-plane exposure to radiance in the scene. We used a calibrated reference source (Labsphere CSTM-USS-1200) to measure each of these camera characteristics.

To measure the OECF, we removed the camera lens to expose the CCD sensor directly to the source. We used a variable iris aperture and individual control of the four lamps in the source to vary irradiance through a range of more than 1600:1. A previously calibrated digital camera was used as a reference.

To measure the flat-field response, we remounted the lens (which is the principle source of flat-field variation) and took a series of exposures with the source appearing at various positions on the image plane. By fitting a biquadratic function to these images, we approximated the spatial variation across the image plane and were able to compensate for it. This procedure differs from that used previously [18 (Appendix A)] in order to reduce flare associated with the lens used here.

To determine the irradiance at each location on the surface, we approximated the source as a single point.³ In order for this model to be valid, the source must be small compared to the distance to the sample, and its angular intensity distribution must be uniform. We measured the angular distribution of the source by capturing calibrated images of a flat, uniform surface illuminated by the flash and verified that, with an additional diffuser, it is sufficiently uniform over the range of angles we use. To get the absolute magnitude of the BRDF correct, we measured the intensity of the light source relative to the camera’s three color sensitivities by photographing a diffuse white reference sample (a calibrated Spectralon target from Labsphere, Inc.) in a known position.

5.2 Data processing

Processing the measurement images to extract BRDF samples involves two steps. First, the photogrammetric targets are used to determine the geometric arrangement of the sample, camera, source, and reference white target. Second, all this information is given to a *derenderer*, which computes the BRDF values.

³While the real source only approximates a point, compensating for its solid angle requires a deconvolution process that is not trivial. We follow accepted practice of reporting our raw measurements and the solid angle of the source, which is a circle subtending 1.3×10^{-3} steradians. The solid angle of the camera’s aperture, $\approx 6 \times 10^{-5}$ steradians, is negligible by comparison.

We begin by extracting the target positions in each image. This gives us the 2D image positions of the targets visible in each image and their correspondence in different images. This information is used to solve a bundle adjustment system, which computes the poses of all the cameras and the 3D locations of all the targets. It then remains to locate the model of the sample in the same coordinate system. For a cylindrical sample, a cylinder is automatically fit to the 3D locations of the sample targets, which are attached to the sample’s surface. If the sample is a sphere, the user manually specifies points on the boundary of the sample in 3 or 4 images, and a tangent sphere is fit to the corresponding rays to define the sample model. For a sample of arbitrary shape, we scan the sample and the sample targets together. The targets can then be automatically recognized in the luminance image produced from the scan and transformed to their 3D positions within the scan. A rigid-body transformation aligns these scanned 3D positions with the 3D positions of the corresponding targets in the bundle adjustment results, putting the scanned 3D geometry in the same coordinate system as the camera and source positions.

The derenderer is derived from a ray-tracing renderer, and its input is a scene description including the cameras, the light source, and a model of the sample. It uses standard rendering techniques [8] to find the intersection point of each pixel’s viewing ray with the sample surface and to compute the irradiance due to the source. Rather than using a BRDF value to compute the radiance reflected to the pixel, as a renderer would, the derenderer instead divides the pixel’s measured radiance by the irradiance to obtain the BRDF value. The derenderer’s output is a list of BRDF samples, each including the incident direction, the exitant direction, and the BRDF value for that configuration. Separate sample sets are generated from the camera’s red, green, and blue pixels.

If a range scan is providing the model of the sample, the points from the scanner are tessellated to define the surface for ray intersection. To reduce the effects of scanner noise, we derive a normal to compute the BRDF at each point by fitting a plane to a weighted set of nearby points.

6 Results

We have used our image-based system to measure the BRDFs of several materials. Here, we present three materials: matte gray paint, a squash, and human skin. The matte gray paint, applied to a cylinder, allows us to verify that our BRDF measurements are accurate by comparing them with gonireflectometer measurements. The squash and human skin demonstrate the measurement of two surfaces impractical to measure in a traditional gonireflectometer. We have measured other materials ranging from paints to felt, a few of which are shown in rendered images.

For each of the samples, we show measurements in the incidence plane for several values of θ . Plotted with the measurements is a slice of a smooth BRDF reconstructed using local quadratic regression in the BRDF’s 3D domain [5]. This technique defines a smooth, continuous function over the entire BRDF domain that follows the samples and interpolates across unsampled areas. Each curve is a slice of a 3D function fit to all the data points, not just a fit to the points visible with it. Since the curve accounts for more points than are shown, it may sometimes diverge slightly from the points. In these plots, backward scattering is on the left and forward on the right; the specular direction is marked by a vertical gray line.

6.1 Gray cylinder

To verify the correctness of our measurements, we painted a section of aluminum tubing (outside diameter 6 inches) with a sprayed gray primer. The resulting sample has a very uniform surface and is well modeled by an ideal cylinder. We measured its geometry and position using a strip of photogrammetric targets along each edge; a typical measurement image is shown in Figure 4. Because a cylinder curves only along one direction, the resulting data lie very near a two-dimensional slice of the three-dimensional (isotropic) BRDF domain; this allows us to concentrate our measurement points on the incidence plane.

Figure 6 summarizes the results of the gray cylinder measurement. Note the low noise and broad coverage—the results seem reliable out to at least 80° . The raw points shown include measurements both in the forward direction (all θ_e for the θ_i indicated on each plot) and in the reciprocal direction (all θ_i for the indicated θ_e): the scatter shown includes any deviations from reciprocity. The low scatter serves as a first validation of our measurements, since the reciprocal measurements are independent.

We measured a matching flat sample using a gonireflectometer [6] designed according to ASTM recommendations [1] and verified to an accuracy of 5%. The gonireflectometer results are plotted with a dashed line. Note the good correspondence to our image-based measurements; this independent measurement further validates the correctness of our method.

6.2 Squash

Having verified the accuracy of our technique, we applied it to more interesting objects. One of these, a squash, illustrates some of the strengths of our method. There is no practical way to obtain a flat sample of this surface to use in a traditional gonireflectometer.

A typical measurement image is shown in Figure 5. Below the squash, one can see the support structure containing the sample targets (see Section 5.1); the stationary targets can be seen above it. Figure 5 also indicates the approximate subset of the geometry used in the derendering process. The top was truncated by the limits of our 3D scanner; we deleted the lower part to reduce computation time and storage demands. Even this small subset of the available data results in over 300,000 BRDF samples per channel.

The first column of Figure 7 shows the coverage obtained with this sample. The dots are plotted in a polar coordinate system, with radius indicating θ_e or θ_i and angle indicating $\Delta\phi$ ($\Delta\phi = 0$ is at the bottom; the incidence plane, where $\Delta\phi = 0$ or 180° is marked by the vertical line). We include both the forward measurements (fixed θ_i) and reciprocal measurements (fixed θ_e); reciprocity allows us to use these points to help fill the hemisphere. The points in each plot fall on rings, each consisting of samples from one measurement image. The rings appear because the angle between the illumination and viewing direction is nearly constant within each image. There are never any data within a small circle around the incident direction because we cannot physically place the camera at the source position to measure exact retroreflection.

Because of the squash’s compound curvature, much of the BRDF domain is sampled. There are some gaps in the coverage; had we scanned the entire rounded end of the squash, we would have covered the entire hemisphere well. The reconstructed curves in the incidence-plane plots (Figure 7, second column) show that the dataset as a whole defines a smooth function that describes an interesting and plausible BRDF, with an off-specular forward scattering lobe but also a non-Lambertian base color. The data

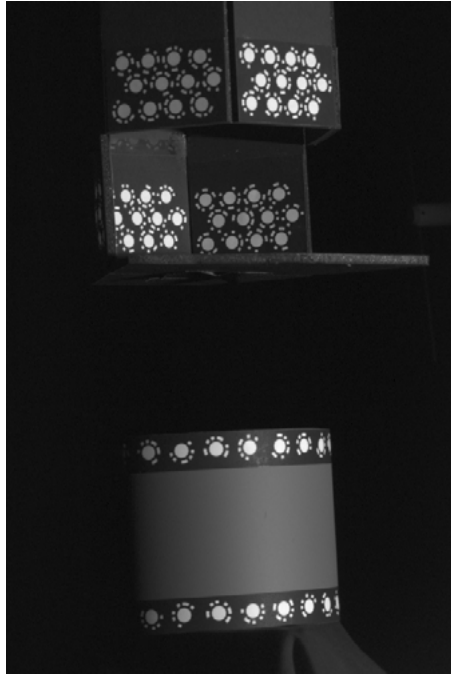


Fig. 4. A typical measurement image from the gray cylinder dataset.

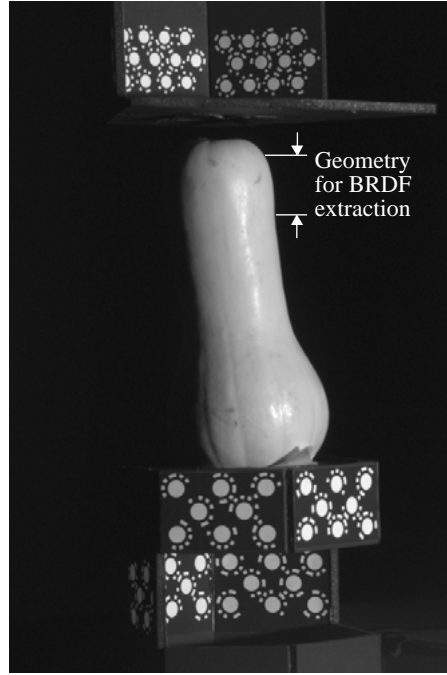


Fig. 5. A typical measurement image from the squash dataset.

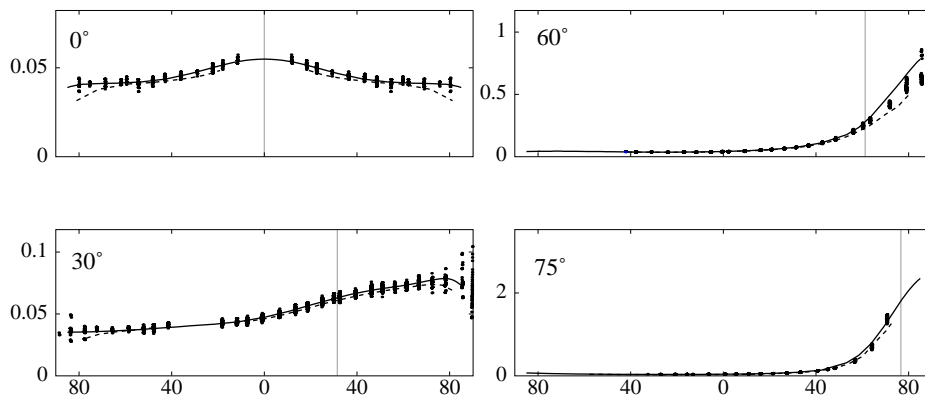


Fig. 6. Summary of results from 29 images of the gray cylinder. Points: raw measurements including reciprocal data. Solid line: local polynomial fit. Dashed line: gonioreflectometer results.

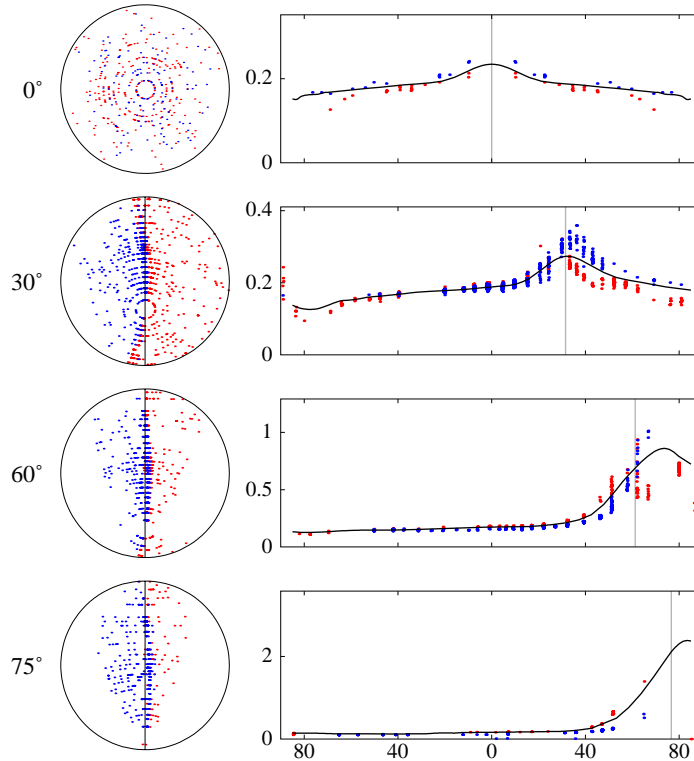


Fig. 7. Summary of results for the squash dataset. Left column: sample coverage; right column: raw data and local polynomial fit.

contain considerably more noise than do the gray cylinder data, as might be expected given the irregular nature of the surface, the noise in the 3D scanner data, and the finite precision of aligning the scanner data with the images. The slight surface blemishes visible in Figure 5 will affect the scatter plots, but have much less influence on the smoothed BRDF, as they cover only a small fraction of the surface.

6.3 Renderings

Plate 1 (see Appendix) shows some visual results of our reflectance measurements. To condense the data for tractable rendering times, the measurements were approximated with the representation presented by Lafortune et al. [16], using three cosine lobes (besides the diffuse term) for each BRDF.⁴ Of course, the same data could be used in more sophisticated representations or for studies of surface optics and development of new parametric models.

The scene is rendered with Monte Carlo path tracing. It is illuminated by one overhead light source and two smaller light sources in the background, one on each side of the scene. All object surfaces show reflectances measured by our method: gray primer

⁴Because local polynomial reconstruction is slow and difficult to use for stochastic sampling, we did not use it for the renderings.

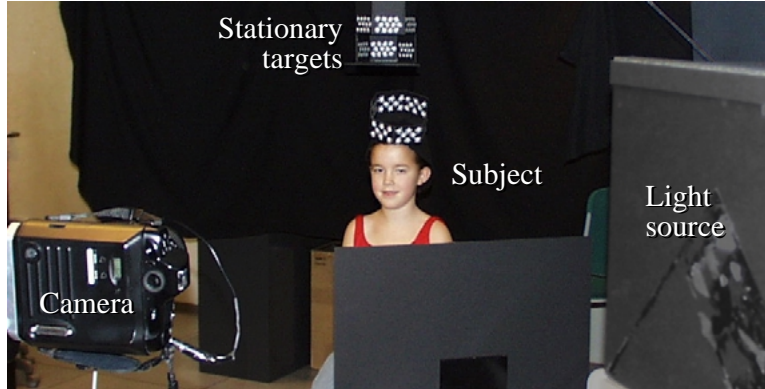


Fig. 8. Measurement setup.

on the floor, an unglazed ceramic on the flowerpot, blue and metallic red paints on the puzzle, and black felt on the hat. Even those surfaces that seem Lambertian in this image display distinctive directional behavior; the floor, for example, shows no visible shadows from the back lights in a Lambertian approximation.

6.4 Human skin

We adapted our method to measure the skin of human subjects. To our knowledge, our measurements are only the second angle-resolved reflectance measurements of living human skin; Cader and Jankowski have used a gonireflectometer-like device to measure UV reflectance [2]. Our method, however, obtains many more BRDF samples in a short time (typically 20 minutes).

To accommodate a human subject, we attached our sample targets to a baseball cap worn backward by the subject. This fixes a field of targets to the subject’s head; the geometry of the targets and the head together is obtained, as before, with the 3D range scanner. We selected a section of the forehead for derendering because it presents a relatively smooth, convex, uniform area of skin that is unlikely to deform during the measurement session. The hat positions the targets so as to make it easy to capture the forehead and all targets in each image.

Since the sample targets are no longer stationary, the stationary targets shown in Figure 8 provide a frame of reference for the positions of the camera, the subject, and the light source. Transforming everything into this frame for derendering allows us to accommodate minor movement of the subject’s head without loss of measurement accuracy.

We measured skin BRDFs from several different subjects. Figure 9 shows coverage and incidence-plane slices of one of our data sets. Scatter is remarkably low, given the difficulties of precise geometric alignment and extracting reliable normals from noisy geometric data.

The BRDF itself is quite unusual; at small incidence angles it is almost Lambertian, but at higher angles strong forward scattering emerges. Note that the scale changes by a factor of 25 from the top row to the bottom. This scattering does not seem to correlate with the specular direction, so it cannot be simulated with a Phong function, nor would it be predicted by traditional rough-surface models such as those of Torrance and Sparrow [22] or He [13]. The only predictive model that might match these data is

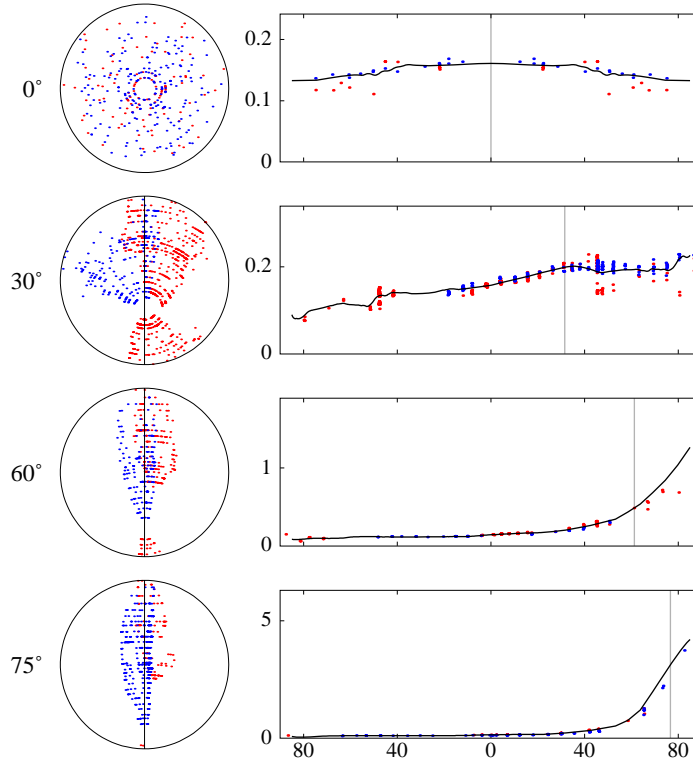


Fig. 9. BRDF of typical skin, showing coverage and scatter in raw data

the Monte Carlo simulation of Hanrahan and Krueger [11]; our data could be used to confirm or refine that method.

The renderings of Plate 2 (see Appendix) show the two extremes of our measurements to date: the BRDFs of a 43-year-old Caucasian male and a 23-year-old male from India, who exhibits not only a different skin color but also noticeably glossier skin.

7 Conclusion

This paper has described a simple technique that can measure the BRDFs of many materials using only a digital camera and a light source. We achieve accuracy rivaling that of a specialized gonireflectometer but with much greater speed and resolution, and with one twentieth the equipment cost. In addition, the technique is versatile enough to measure living human skin. The technique is rapid because the two dimensions of a camera image sample two angular degrees of freedom instantaneously, leaving only one to be handled by sequential measurement. In a measurement session lasting under half an hour, our system can acquire hundreds of thousands of samples scattered over the full domain of an isotropic BRDF. The resulting data are internally consistent and agree closely with independent measurements.

Our technique demands samples with homogeneous BRDF, as do most traditional gonireflectometers and almost all image-based techniques. We also require convex

curved samples; this complements the capabilities of more conventional methods, which only work with flat samples. Just as some materials are most readily available as flat samples (e.g. various building materials), others, including most organic objects, are only available in curved samples.

Acknowledgments

The authors were supported by the National Science Foundation Science and Technology Center for Computer Graphics and Scientific Visualization (ASC-8920219) and by NSF Grant ASC-9523483. Dr. Marschner was also partly supported by the Hewlett-Packard Corporation, who also donated several of the workstations used in this work. In addition, we thank HP Laboratories for accommodating Dr. Marschner's work on this paper during his employment there. Measurement equipment was provided by NSF grant CTS-9213183 and by the Imaging Science Division of the Eastman Kodak Company. Special thanks to Grace Westin, Sebastian Fernandez, and Mahesh Ramasubramanian, who served as additional test subjects for skin BRDF measurements.

References

1. Standard practice for angle resolved optical scatter measurements on specular or diffuse surfaces. ASTM Standard E 1392-96.
2. A. Cader and J. Jankowski. Reflection of ultraviolet radiation from different skin types. *Health Physics*, 74(2):169–172, February 1998.
3. Raymond J. Castonguay. New generation high-speed high-resolution hemispherical scatterometer. In John C. Stover, editor, *SPIE Proceedings*, volume 1995, pages 152–165, July 1993.
4. J. H. Chandler and C. J. Padfield. Automated digital photogrammetry on a shoestring. *Photogrammetric Record*, 15(88):545–559, 1996.
5. J. Fan and I. Gijbels. *Local Polynomial Modeling and Its Applications*. Chapman and Hall, London, 1996.
6. Sing-Choong Foo. A gonireflectometer for measuring the bidirectional reflectance of material for use in illumination computation. Master's thesis, Cornell University, 1997.
7. C. S. Fraser, M. R. Shortis, and G. Ganci. Multi-sensor system self-calibration. In *Video-metrics IV*, pages 2–18. SPIE, October 1995.
8. A. Glassner, editor. *An Introduction to Ray Tracing*. Academic Press, London, 1989.
9. Steven J. Gortler, Radek Grzeszczuk, Richard Szeliski, and Michael F. Cohen. The lumigraph. In *Computer Graphics (SIGGRAPH '96 Proceedings)*, pages 43–54, August 1996.
10. Anat Grynberg and Greg Ward. A new tool for reflectometry. Monograph 161, Lawrence Berkeley Laboratory, July 1990.
11. Pat Hanrahan and Wolfgang Krueger. Reflection from layered surfaces due to subsurface scattering. In *Computer Graphics (SIGGRAPH '93 Proceedings)*, pages 165–174, August 1993.
12. Ziad R. Hatab, John R. McNeil, and S. Sohail H. Naqvi. Sixteen-megabit dynamic random access memory trench depth characterization using two-dimensional diffraction analysis. *Journal of Vacuum Science and Technology B*, 13(2):174–181, March/April 1995.
13. Xiao D. He, Kenneth E. Torrance, Francois X. Sillion, and Donald P. Greenberg. A comprehensive physical model for light reflection. *Computer Graphics (SIGGRAPH '91 Proceedings)*, 25(4):175–186, July 1991.
14. Katsushi Ikeuchi and Kosuke Sato. Determining reflectance properties of an object using range and brightness image. *IEEE Transactions on Pattern Analysis and Machine Intelligence*, 13(11):1139–1153, 1991.

15. Konrad F. Karner, Heinz Mayer, and Michael Gervautz. An image based measurement system for anisotropic reflection. *Computer Graphics Forum (Eurographics '96 Proceedings)*, 15(3):119–128, August 1996.
16. Eric P. F. Lafortune, Sing-Choong Foo, Kenneth E. Torrance, and Donald P. Greenberg. Non-linear approximation of reflectance functions. In *Computer Graphics (SIGGRAPH '97 Proceedings)*, pages 117–126, August 1997.
17. Rong Lu, Jan J. Koenderink, and Astrid M. L. Kappers. Optical properties (bidirectional reflectance distribution functions) of velvet. *Applied Optics*, 37(25):5974–5984, September 1998.
18. Stephen R. Marschner. *Inverse Rendering for Computer Graphics*. PhD thesis, Cornell University, 1998.
19. F. E. Nicodemus, J. C. Richmond, J. J. Hsia, I. W. Ginsberg, and T. Limperis. Geometric considerations and nomenclature for reflectance. Monograph 160, National Bureau of Standards (US), October 1977.
20. Yoichi Sato, Mark D. Wheeler, and Katsushi Ikeuchi. Object shape and reflectance modeling from observation. In *Computer Graphics (SIGGRAPH '97 Proceedings)*, pages 379–387, August 1997.
21. K. E. Torrance and E. M. Sparrow. Off-specular peaks in the directional distribution of reflected thermal radiation. *Transactions of the ASME*, 88:223–230, May 1966.
22. K. E. Torrance and E. M. Sparrow. Theory for off-specular reflection from roughened surfaces. *Journal of Optical Society of America*, 57(9):1105–1114, 1967.
23. Gregory J. Ward. Measuring and modeling anisotropic reflection. *Computer Graphics (SIGGRAPH '92 Proceedings)*, 26(2):265–272, July 1992.

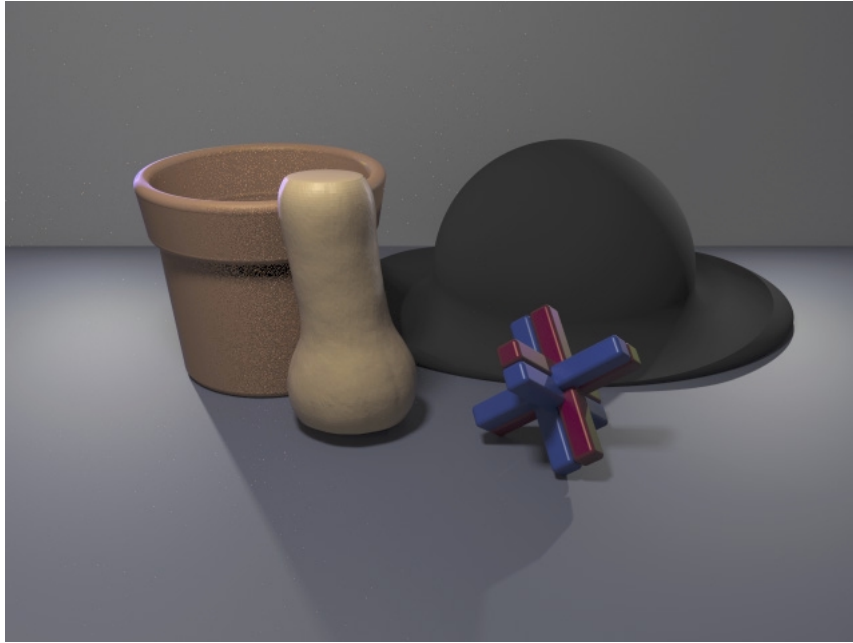


Plate 1. A rendered image showing a scene containing objects made of the measured materials.

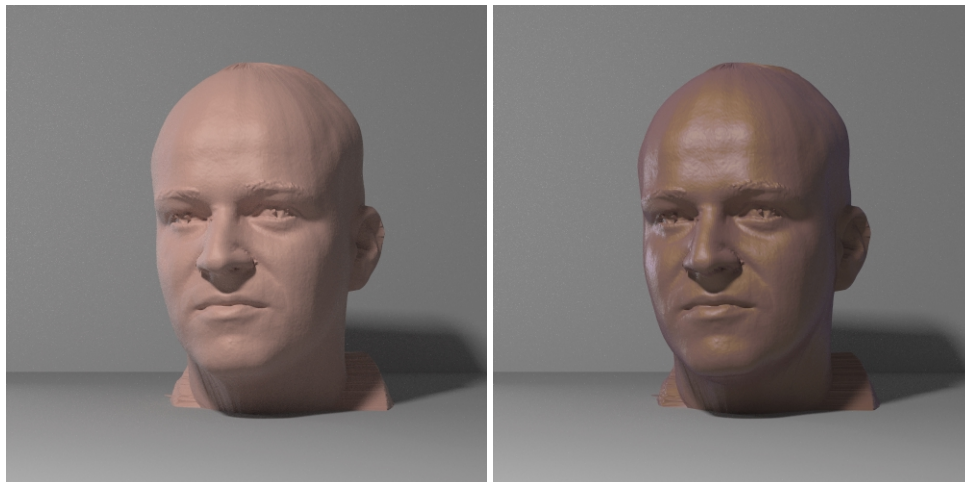


Plate 2. Rendered images showing BRDFs measured from two different subjects.